Article

High-Performance FAU Zeolite Membranes Derived from Nano-Seeds for Gas Separation

Qing Wang *, Huiyuan Chen , Feiyang He , Qiao Liu , Nong Xu , Long Fan , Chuyan Wang , Lingyun Zhang , Rongfei Zhou *

Posted Date: 19 October 2023

doi: 10.20944/preprints202310.1150.v1

Keywords: FAU membrane; zeolite; secondary growth; gas separation; propylene propane separation; H2/C3H8 separation

Article

High-Performance FAU Zeolite Membranes Derived from Nano-Seeds for Gas Separation

Qing Wang [1,2,*], Huiyuan Chen [1], Feiyang He [1], Qiao Liu [1], Nong Xu [1], Long Fan [1], Chuyan Wang [3], Lingyun Zhang [1] and Rongfei Zhou [2,*]

[1] School of Energy, Materials and Chemical Engineering, Hefei University, Hefei 230601, China
[2] State Key Laboratory of Materials-Oriented Chemical Engineering, College of Chemical Engineering, Nanjing Tech University, Nanjing 210009, China
[3] School of Biological Food and Environment, Hefei University, Hefei 230601, China
* Correspondence: qingwang@hfuu.edu.cn (Q.W.); rf-zhou@njtech.edu.cn (R.F.Z.)

Abstract: In this study, high-performance FAU (NaY type) zeolite membranes were successfully synthesized using small-sized seeds of 50 nm, and their gas separation performance was systematically evaluated. Employing nano-sized NaY seeds and an ultra-dilute reaction solution with a molar composition of 80 Na_2O: 1Al_2O_3: 19 SiO_2: 5000H_2O, the effects of synthesis temperature, crystallization time, and porous support (α-Al_2O_3 or mullite) on the formation of FAU membranes were investigated. The results illustrated that further extending the crystallization time or increasing the synthesis temperature led to the formation of a NaP impurity phase on the FAU membrane layer. The most promising FAU membrane with a thickness of 2.7 μm was synthesized on an α-Al_2O_3 support at 368 K for 8 h, and had good reproducibility. The H_2 permeance of the membrane was as high as 5.34×10^{-7} mol/(m^2 s Pa), and the H_2/C_3H_8 and H_2/i-C_4H_{10} selectivities were 183 and 315, respectively. The C_3H_6/C_3H_8 selectivity of the membrane was as high as 46 with a remarkably high C_3H_6 permeance of 1.35×10^{-7} mol/(m^2 s Pa). The excellent separation performance of the membrane is mainly attributed to the thin, defect-free membrane layer and relatively wide pore size (0.74 nm).

Keywords: FAU zeolite membrane; molecular sieve membrane; secondary growth; gas permeation; propylene propane separation; H_2/C_3H_8 separation

1. Introduction

The high energy consumption of gas separation has become one of the important environmental issues with the seriousness of global climate change, because the increase in traditional energy consumption will lead to an increase in CO_2 emissions. Sholl et al. pointed out that the separation of alkenes from alkanes is one of the "seven chemical separations to change the world" [1]. The separation and purification of propylene and ethylene alone accounts for 0.3% of global energy use. Among them, propylene has long been one of the important chemical raw materials due to the wide application of its downstream products in the chemical and petroleum industries. Currently, propylene/propane separation is mainly performed by cryogenic distillation. However, it is a great challenge to separate propylene from propane since the boiling points of propylene (225.7 K) and propane (231 K) are close, and the distillation process requires a large tower with 150-300 stages and a high reflux ratio [2]. The significant energy requirements and capital costs of cryogenic distillation processes have prompted research into other methods to separate these gases. Membrane-based gas separation is an attractive and forward-looking technology because it can be performed under mild conditions without phase changes, and can be completed in one step, which can significantly reduce energy consumption by up to 80% with the related carbon footprint [3,4].

Various membrane materials, such as polymer membranes [5,6], zeolite membranes [3,7,8], metal-organic framework (MOF) membranes [9,10], mixed matrix membranes [11,12], and silicon

Preprints (www.preprints.org) | NOT PEER-REVIEWED | Posted: 19 October 2023 doi:10.20944/preprints202310.1150.v1

carbide membranes [13-15], have been explored for separation. Among them, zeolites have become promising candidates for high-performance membranes in separation processes, catalytic membranes, and sensors, considering their well-defined pore size, molecular sieving performance, high thermal stability, and high mechanical strength [16]. To date, much effort has been devoted to developing fine zeolite membranes. The FAU-type zeolite (including NaX with Si/Al ratio ≤ 1.5, and NaY with Si/Al ratio >1.5) membranes with a pore diameter of 0.74 nm are suitable for separating large molecules that cannot be effectively handled by MFI (0.55 nm), LTA (0.42 nm) and CHA (0.38 nm) zeolite membranes. FAU membranes have been used in liquid separation (pervaporation), gas separation, and ion removal [17]. Combining the large pore size and affinity of FAU zeolites endows the membrane with high flux and selectivity [18].

So far, two typical methods for synthesizing supported FAU membranes have been developed [19]. The first method is in-situ growth; that is, the porous support is immersed in the synthesis solution, and then the required membrane layer is grown directly on the surface of the support by hydrothermal synthesis. Although this method is very simple, forming a pure phase and dense FAU membrane is difficult due to the poor heterogeneous nucleation of FAU crystal nuclei on the support surface during the in-situ growth process [20]. The second widely used strategy for FAU membrane synthesis is secondary growth. The secondary growth includes depositing seed crystals on the support surface via rub coating, dip coating, or vacuum suction, followed by secondary hydrothermal synthesis [21]. The secondary growth has many advantages compared to in-situ crystallization methods. It facilitates control of the membrane microstructure (e.g., thickness and orientation). In particular, the seed layers can weaken the impact of the support, reduce defects, and achieve high reproducibility [18].

Over the past decades, FAU membranes have received extensive attention from researchers [22]. Shrestha et al. synthesized a continuous FAU membrane on a porous polyethersulfone support by secondary growth; the membrane exhibited a selectivity of 2.4 ± 0.8 for C_3H_6/C_3H_8 with a C_3H_6 permeance of (4.05 ± 1.86) × 10^{-7} mol/(m^2 s Pa). Gu et al. synthesized dense FAU membranes on porous α-alumina (α-Al_2O_3) supports using FAU seeds with 1-1.5 μm sizes [23]. The membrane had a thickness of 4 μm and exhibited CO_2 selectivity with a separation factor of 31.2 for the CO_2/N_2 dry gas mixture and a CO_2 permeance of 2.1 × 10^{-8} mol/(m^2 s Pa). Zhou et al. prepared an FAU membrane with a thickness of ~2.3 μm on polydopamine (PDA)-modified α-Al_2O_3 support through in-situ growth [19]. The membrane showed H_2/CH_4 and H_2/C_3H_8 separation factors of 9.9 and 127.7, respectively, and exhibited H_2 permeance as high as 1.9× 10^{-7} mol/(m^2 s Pa). However, the support modification process was relatively complex, and the expensive PDA further limited the large-area preparation of the membrane. Recently, Nazir et al. systematically investigated the effect of FAU seed size (0.75-5.5 μm) on the formation of FAU membranes on α-Al_2O_3 supports [22]. Their results showed that the growth of the membrane layer was enhanced, and the membrane defects were successfully reduced by using smaller seed particles of 750 nm, which is attributed to the minimal gaps between the seed particles. However, the size of the seeds (750 nm) was still large for obtaining high-quality, defect-free FAU membranes. Furthermore, an impurity phase NaP is easily formed in the zeolite layer during the FAU membrane synthesis, making it difficult to prepare a pure-phase FAU membrane.

As mentioned above, the synthesis of high-performance FAU zeolite membranes still faces challenges, such as the formation of intercrystalline defects, impure phases, and poor reproducibility. Many parameters could influence the formation of FAU membranes, such as gel composition, aging conditions, hydrothermal temperature and time, as well as easily overlooked support properties and seed size. Understanding the influence of these parameters is important to control the synthesis process and producing high-performance FAU membranes. This work used nano-sized FAU seeds to explore the effects of crucial parameters (i.e., hydrothermal temperature and time) on the formation of FAU membranes on α-Al_2O_3 and mullite supports, respectively. High-performance FAU membranes were prepared by carefully tuning synthesis parameters to obtain optimal formation conditions. The as-prepared membranes exhibited excellent separation performance for H_2/C_3H_8 and C_3H_6/C_3H_8.

Preprints (www.preprints.org) | NOT PEER-REVIEWED | Posted: 19 October 2023 doi:10.20944/preprints202310.1150.v1

2. Experimental

2.1. Materials

All procedures were performed under an ambient atmosphere unless otherwise stated. All reagents were obtained from commercial suppliers and used without further purification: Ludox HS-30 colloidal silica (SiO_2/Na_2O= 90, 30 wt% suspension in H_2O, Aldrich); tetramethylammonium hydroxide (TMAOH, 25 wt% in H_2O, Aldrich); aluminum isopropoxide ($Al(O\text{-}i\text{-}Pr)_3$, 98 wt%, Aldrich); tetramethylammonium bromide (TMABr, 99 wt%, Aladdin); sodium aluminate ($AlNaO_2$, Al/NaOH=0.79, Wako); sodium hydroxide (NaOH, 97 wt%, Aladdin); sodium silicate solution (reagent grade, SiO_2=26.5 wt%, Na_2O=10.6 wt%, Aldrich); porous α-Al_2O_3 (average pore diameter: 200 nm, outer diameter: 12 mm, length: 6 cm) and mullite (average pore diameter: 1.3 μm, outer diameter: 12 mm, length: 6 cm) tube supports were provided by Nanjing Tech University. The preparation procedure of nano-sized NaY seeds and Nay-type zeolite FAU membranes was summarized in Figure 1.

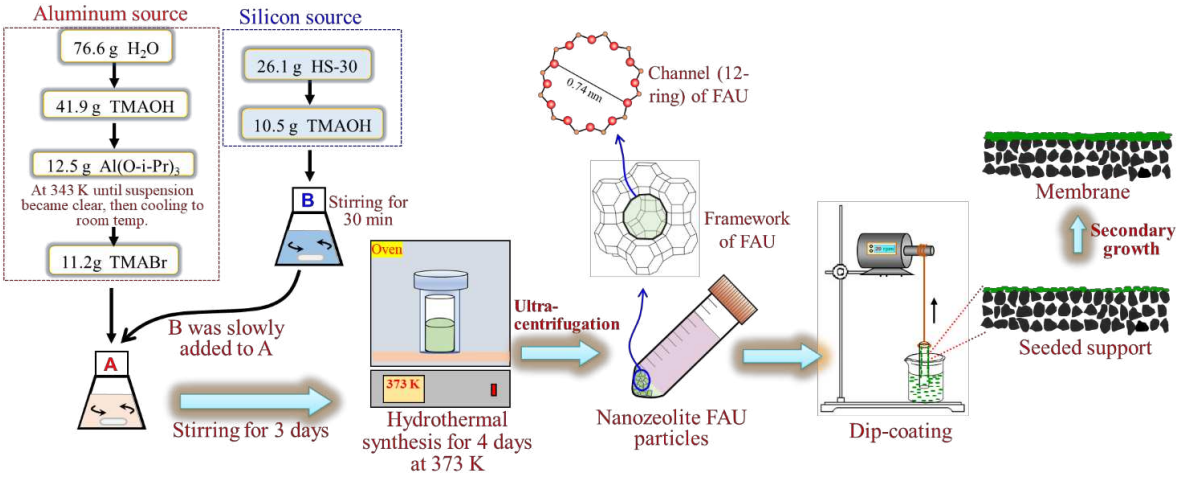

Figure 1. Schematic illustrations of the hydrothermal synthesis of nano-sized FAU seeds and membranes.

2.2. Synthesis of nano-NaY seeds

Nano-sized NaY seeds were synthesized according to the literature [24] with slight modifications. The silicon and aluminum sources were prepared separately before mixing. Typically, the molar composition of the silicon source was $0.048Na_2O$: $4.35SiO_2$: 0.96TMAOH: $48.46H_2O$; that is, 26.2g Ludox HS-30 colloidal silica and 10.46g TMAOH were mixed and stirred at room temperature for 30 min. The molar composition of the alumina source was $1Al_2O_3$: 3.84TMAOH: 2.4TMABr: $200.54H_2O$. 76.6 g H_2O and 41.9 g TMAOH were mixed, and 12.5 g $Al(O\text{-}i\text{-}Pr)_3$ was dissolved in this mixture while stirring in a water bath at 343 K until the suspension became clear. After cooling to room temperature, 11.2 g TMABr was added to the mixture and stirred at room temperature for 15 min. Then, the silica source was slowly added to the aluminum source while stirring. The final molar composition of the nano-sized NaY synthesis solution was $0.048Na_2O$: 4.80TMAOH: 2.4TMABr: $4.35SiO_2$: $1.0Al_2O_3$: $249H_2O$. The clear solution was aged with stirring at room temperature for 3 days, then transferred into a Teflon-lined autoclave and heated in an oven at 373 K for 4 days. In the product mixture, nano-sized NaY particles were captured using an ultracentrifuge and washed with distilled water until pH 7. Finally, the seeds were dispersed in water to obtain a 1 wt% seed suspension.

2.3. Synthesis of FAU (NaY) membrane

FAU (NaY) zeolite membranes were hydrothermally synthesized on the outer surface of tube supports. As reported previously [3], the NaY seeds were coated on the outer surface of the tubular support via a dip-coating technique. Before seeding, both ends of the tubular support were sealed

Preprints (www.preprints.org) | NOT PEER-REVIEWED | Posted: 19 October 2023 doi:10.20944/preprints202310.1150.v1

with silicone plugs to prevent the inner surface from coating with seeds. The dried tubular supports were immersed in the seed suspension for 60 s and subsequently dried at 373 K for 15 min.

The molar composition used for membrane growth was 80Na_2O: 1Al_2O_3: 19SiO_2: 5000H_2O, and the specific procedure was described below. $AlNaO_2$ was added to a mixed solution of deionized water and NaOH while stirring at room temperature for 0.5 h. Sodium silicate solution was added to the above solution while stirring for 12 h, then transferred into a Teflon-lined autoclave. The seeded tubular supports were placed vertically in an autoclave and fully immersed in the gel. Hydrothermal synthesis was done in an oven at 358-378 K for 3-10 h. After crystallization, the synthesized membranes were removed from the solution, washed with water, and dried at 333 K.

2.4. Characterization and gas permeation

The morphology and Si/Al ratio of seeds and membranes were observed using a Hitachi S-4800 scanning electron microscope (SEM) coupled with an energy-dispersive X-ray (EDX) analyzer. The crystalline phases of seeds and membranes were identified by X-ray diffraction (XRD, Ultima IV) using Cu Kα radiation in the 2θ range from 5 to 45°. Before gas permeation measurement, the membrane was placed in a vacuum oven at 373 K overnight to remove water from the zeolite pores. Single-gas permeation performance of FAU membranes was evaluated at room temperature using an experimental setup schematically shown elsewhere [25,26]. Single gases (H_2, 0.289 nm; CO_2, 0.33 nm; N_2, 0.364 nm; CH_4, 0.38 nm; C_3H_6, 0.47 nm; C_3H_8, 0.51 nm, and *i*-C_4H_{10}, 0.53 nm) with different kinetic diameters were fed to the outside of the cylindrical membrane. The feed gas was pressurized at ~0.4 MPa (except for *i*-C_4H_{10}, which was at 0.1 MPa), while the permeate stream was maintained at atmospheric pressure. The permeate flow rate was measured via a soap-film meter. The selectivity is defined as the permeance ratio of single gases [27,28].

3. Results and discussion

3.1. Characterization of FAU seed and seed layer

Figure 2 shows the XRD pattern and SEM image of the as-synthesized FAU seeds. The XRD pattern (Figure 2a) of the as-synthesized zeolite sample shows a series of characteristic peaks at 2θ= 6.2°, 10.1°, 15.58°, 18.62°, 23.54°, and 31.27°, which matched well with the standard FAU, indicating that the seed crystals were pure FAU. The SEM image (Figure 2b) shows that the zeolite particle morphology was roughly spherical, with an average particle size of approximately 50 nm. The Si/Al ratio of the seed crystals was 1.9 by the EDX analysis, which is within the Si/Al range of NaY zeolite. Therefore, nano-sized NaY seeds with pure phase were successfully synthesized.

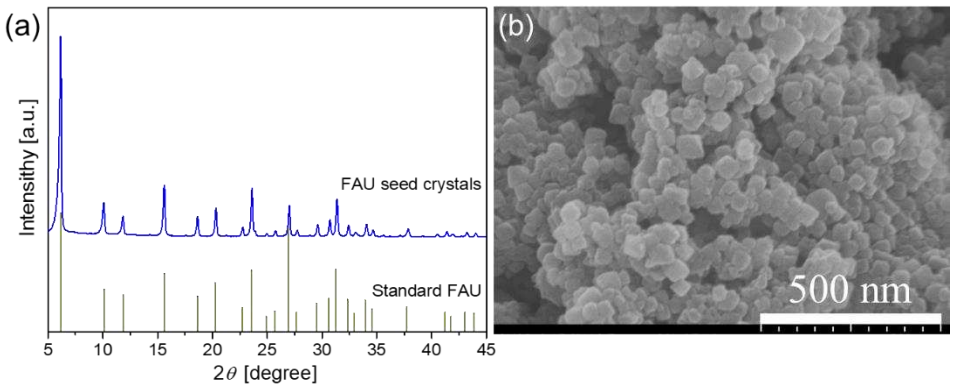

Figure 2. (a) XRD pattern and (b) SEM image of the as-synthesized FAU seeds.

Some seeding methods have been used to prepare zeolite membranes, among which the dip-coating method is simpler. Figure 3 shows the surface, and cross-sectional SEM images of the seeded α-Al_2O_3 and mullite supports via dip-coating. It was observed that the surface of the porous α-Al_2O_3 support was completely covered with a uniform, smooth, densely-packed FAU seed layer with a

 doi:10.20944/preprints202310.1150.v1

thickness of approximately 1.4 μm. The surface of the porous mullite support was also completely covered with a uniform FAU seed layer with a thickness of ~1.1 μm. However, the seed layer on mullite support exhibited obvious cracks, which could be attributed to the high roughness of the microporous (1.3 μm) mullite surface. In addition, it can be observed from the cross-sectional SEM images of the seeded supports that the seeds had not penetrated the internal pores of the α-Al_2O_3 support; on the contrary, the seeds penetrated the mullite support and filled the internal pores (highlighted in red line in Figure 3d), and there was no obvious boundary between the seed layer and the support. Different supports will impact the microstructure and properties of FAU membranes, as will be discussed later when describing the synthesis of the membranes.

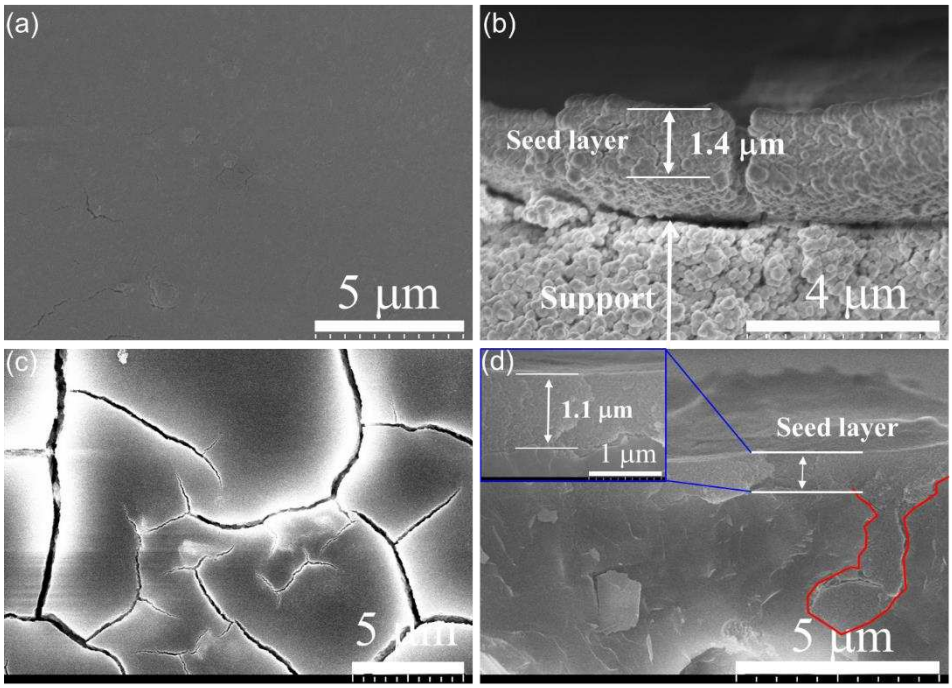

Figure 3. Surface (a, c) and cross-sectional (b, d) SEM images of seeded α-Al_2O_3 (a, b) and mullite supports (c, d).

3.2. Membrane synthesis under different conditions

The preparation of zeolite membranes is affected by many factors, among which reasonable control of temperature and crystallization time is crucial to prepare pure FAU zeolite membranes and avoid the formation of impurity phases. In this study, FAU membranes were prepared by hydrothermal synthesis at 358-378 K for 3-10 h by immersing the seeded supports in an ultra-dilute solution with a molar composition of $80Na_2O$: $1Al_2O_3$: $19SiO_2$: $5000H_2O$. Compared with previous reports [19,23,29], the dilute clear reaction solution had a high water content, which plausibly reduced the nucleation effect in the bulk of the reaction solution and instead promoted crystal growth on the seed layer [21,30].

3.2.1. Effect of synthesis time on membrane formation on α-Al_2O_3 support

Figure 4 shows the XRD patterns of FAU membranes synthesized at 368 K for 3-10 h. It can be observed that the membrane synthesized for 3 h showed weak characteristic peaks of FAU zeolite at 2θ values of 6.2°, 10.1°, 15.58°, 23.54°, and 31.27°, indicating that the crystallinity of the zeolite layer was low. The peak intensity of as-synthesized FAU membranes increased with synthesis time, indicating the growth of the zeolite layer. However, when the synthesis time was prolonged to 10 h, some weak peaks were observed at 2θ= 12.5°, 17.7°, 21.7°, 28.2°, and 33.4°, indicating that NaP zeolite existed in the membrane as an impurity phase [31]. The formation of NaP impurity in preparing FAU zeolite membrane was similar to that of T-type zeolite in preparing LTA zeolite for a long synthesis time [32].

Preprints (www.preprints.org) | NOT PEER-REVIEWED | Posted: 19 October 2023 doi:10.20944/preprints202310.1150.v1

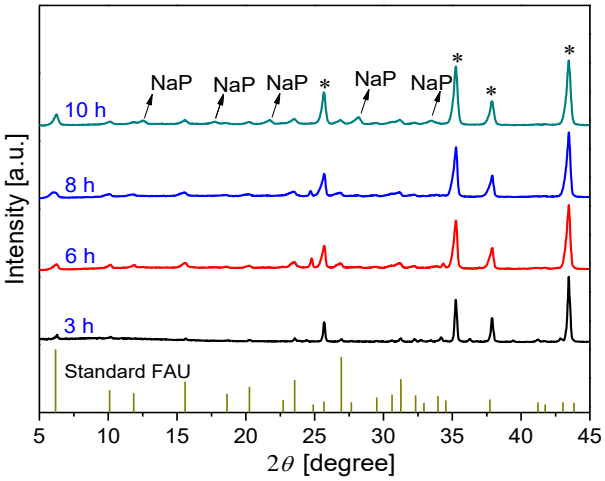

Figure 4. XRD patterns of FAU membranes prepared on α-Al_2O_3 supports at 368 K with different crystallization times (*: α-Al_2O_3 support).

Figure 5 shows the SEM images of FAU membranes synthesized at 368 K for different synthesis times. It can be observed that the membrane synthesized for a crystallization period of 3 h has a loose membrane layer (Figure 5a), and the membrane thickness increased from a 1.4 μm thick seed layer to ~1.9 μm (Figure 5b). Notably, the original seed crystals with a size of 50 nm in the seed layer have grown larger (0.5-1 μm). Still, the crystal morphology was incomplete, indicating that it is not completely crystallized, which is consistent with the XRD results in Figure 4. When increasing the synthesis time to 6 h (Figures 5c and d), the facets (or outlines) of the crystals were slightly clear, but they were loosely connected to each other, and the thickness of the membrane was approximately 2.3 μm. When the synthesis time was extended to 8 h (Figures 5e and f), a continuous, uniform, and dense zeolite layer was formed on the support, and the thickness of the zeolite membrane was about 2.7 μm. When the crystallization time was prolonged to 10 h (Figures 5g and h), a large number of walnut-like crystals appeared on the surface of the zeolite layer. The walnut-like crystals were NaP zeolite according to the XRD pattern (Figure 4). Therefore, the membrane was roughly divided into two layers: the bottom layer was an FAU zeolite layer with a thickness of ~4.8 μm, and the top layer was a NaP layer with a thickness of ~4.1 μm. The presence of NaP crystals in the membrane layer could reduce the membrane permeability due to the smaller pore size of P zeolite (~0.29 nm) and reduce the thermal stability of the membrane due to the cubic-to-tetragonal phase transformation of NaP even at low temperatures [23,33]. The Si/Al ratio of the membrane synthesized at 368 K for 8 h measured by EDX was ~2.1, indicating that the as-synthesized FAU membrane belongs to the NaY type. To avoid impurity phases, the following investigations were conducted with a synthesis time of 8 h.

Preprints (www.preprints.org) | NOT PEER-REVIEWED | Posted: 19 October 2023 doi:10.20944/preprints202310.1150.v1

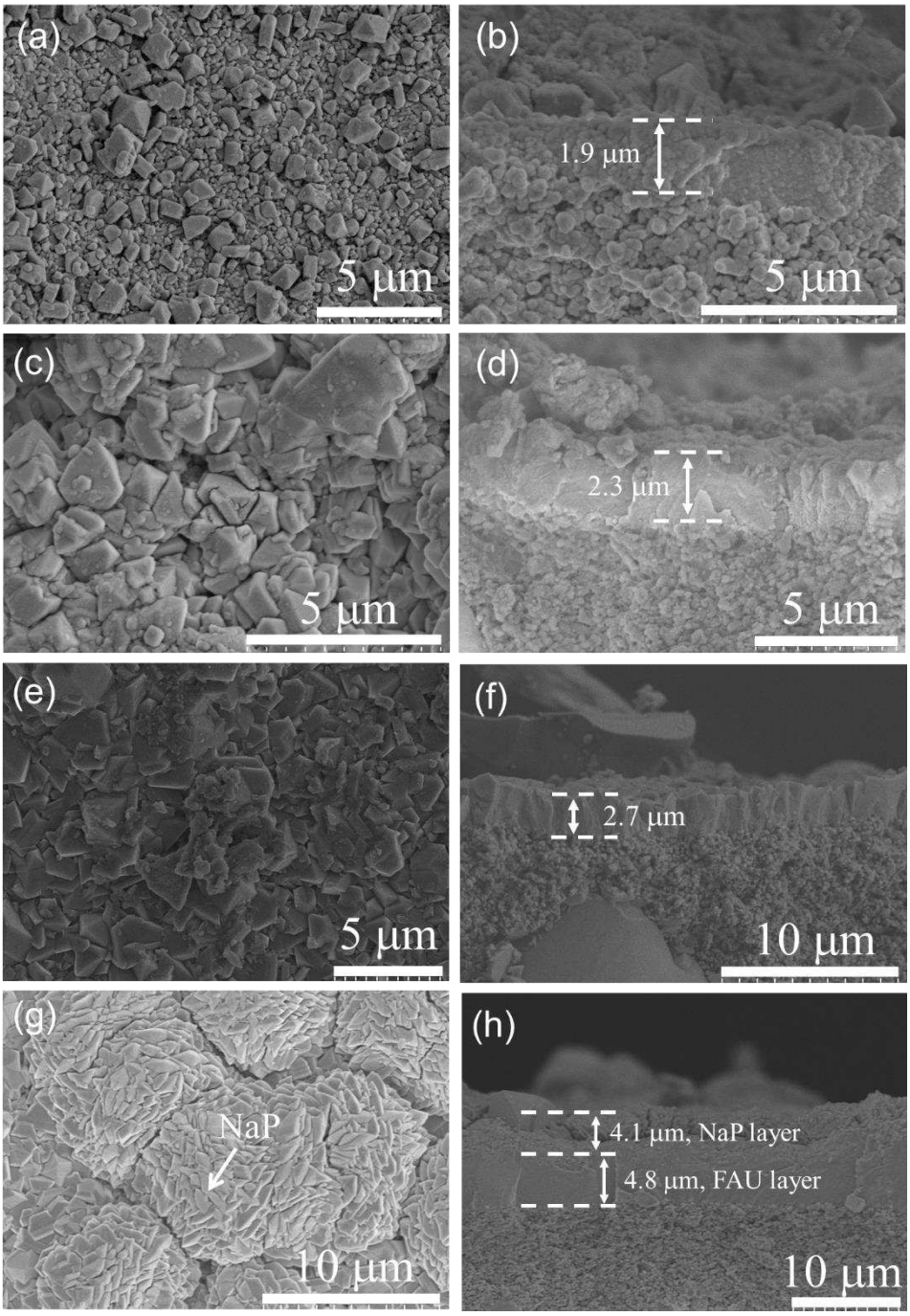

Figure 5. Surface and cross-sectional SEM images of FAU membranes synthesized at 368 K on α-Al_2O_3 supports with different crystallization times. (a, b) 3 h, (c, d) 6 h, (e, f) 8 h, (g, h) 10 h.

3.2.2. Effect of synthesis temperature on membrane formation on α-Al_2O_3 support

Crystallization temperature is an important parameter for forming a specific type of zeolite phase. The hydrothermal synthesis temperature affects the nucleation and crystallization of zeolites, with higher synthesis temperatures leading to higher energy, which is beneficial to the crystallization process [21].

Figures 6 and 7 show the XRD patterns and SEM images of the membranes synthesized at different temperatures for 8 h, respectively. As shown in Figure 6, the intensity of characteristic peaks of the synthesized membranes increased with the synthesis temperature. The membrane synthesized at 358 K for 8 h showed weak FAU characteristic peaks, indicating the formation of FAU zeolite on the support. However, loosely packed small crystals with incomplete shapes formed the membrane-like layer with a thickness of 2.4 μm on the α-Al_2O_3 support (Figure 7). The intensity of characteristic

Preprints (www.preprints.org) | NOT PEER-REVIEWED | Posted: 19 October 2023 doi:10.20944/preprints202310.1150.v1

peaks of the membranes synthesized at 368 K was significantly enhanced. And a pure, fully covered, dense FAU layer was obtained on the α-Al_2O_3 support (as mentioned before). When the synthesis temperature increased to 378 K, the characteristic peaks of NaP appeared in the XRD pattern of the synthesized membrane. The membrane layer included an FAU layer with a thickness of ~4.6 μm and a NaP layer of ~4.2 μm. Those results suggest that the crystallization rate increases with increasing the synthesis temperature; however, the phase transition from the FAU-type zeolite structure to the NaP impurity zeolite structure becomes more significant [34].

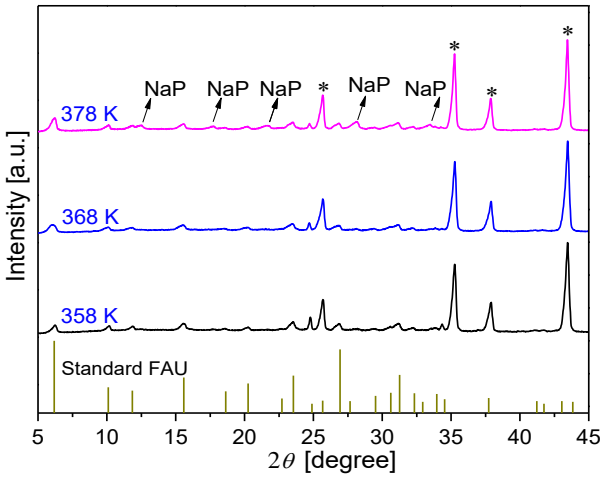

Figure 6. XRD patterns of FAU zeolite membranes prepared on α-Al_2O_3 supports at different crystallization temperatures for 8 h (*: α-Al_2O_3 support).

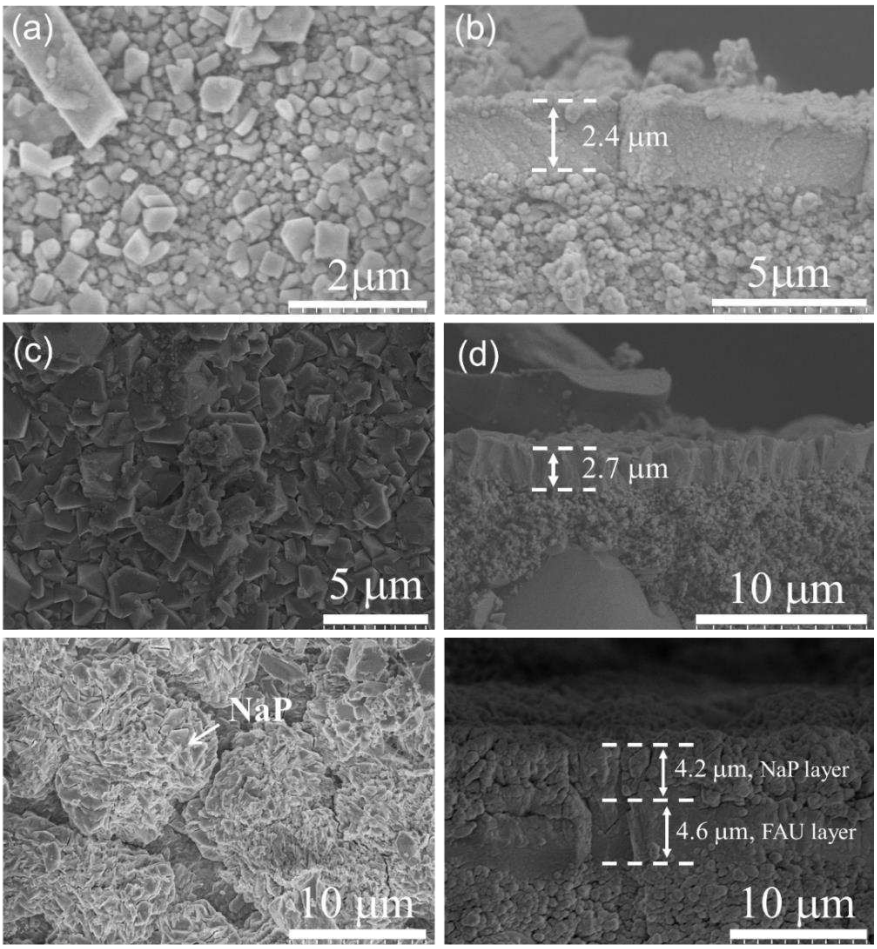

Figure 7. Surface and cross-sectional SEM images of FAU zeolite membranes synthesized on α-Al_2O_3 supports at different crystallization temperatures for 8 h. (a, b) 358 K, (c, d) 368 K, (e, f) 378 K.

Preprints (www.preprints.org) | NOT PEER-REVIEWED | Posted: 19 October 2023 doi:10.20944/preprints202310.1150.v1

3.2.3. Effect of synthesis time on membrane formation on mullite support

Based on the details discussed thus far, employing FAU seeds with a size of 50 nm and an ultra-dilute reaction solution, the effects of synthesis temperature and time on the formation of FAU membranes on α-Al_2O_3 supports were investigated, and the optimized conditions for membrane synthesis were determined to be 368 K for 8 h. In this section, we set the synthesis temperature at 368 K and tried to prepare satisfactory FAU membranes on cheap mullite supports by controlling the crystallization time despite the different pore sizes of the mullite and α-Al_2O_3 supports.

Figures 8 and 9 show the XRD patterns, and SEM images of the membranes synthesized on mullite supports at 368 K for different crystallization times, respectively. As shown in Figure 8, the intensity of characteristic peaks of the synthesized membranes increased with the synthesis time. When the synthesis time increased from 3 to 4.5 h, the intensity of the characteristic peaks of FAU was slightly enhanced, the crystals on the membrane surface were incomplete, and the membrane thickness increased from 1.1 μm (the seed layer) to 5.2 μm (Figures 9a-d). This indicates that the growth of seeds from the seed layer and support pores occurred within 4.5 h of synthesis time.

When the synthesis time increased from 4.5 to 6 h, the intensity of the characteristic peaks of FAU was significantly increased, while that increased slightly from 6 to 8 h. Figures 9e and f show that the membrane layer with a thickness of 7.9 μm was continuous and dense without obvious cracks and holes after 6 h of synthesis. The surface morphology of the membrane synthesized for 8 h was similar to that of the membrane synthesized for 6 h. The main difference was that after 8 h of synthesis, the membrane layer began to grow into the support, increasing the membrane thickness to ~9.2 μm (Figures 9g and h). However, a thick membrane layer increases mass transfer resistance and reduces permeability [35,36]. When the synthesis time was prolonged to 10 h, the characteristic peaks of the NaP impurity phase appeared. Figures 9i and j show that there were many walnut-like NaP crystals on the membrane surface, and the growth of the membrane layer towards the interior of the support became more severe, resulting in the membrane thickness increasing to ~22 μm. The Si/Al ratio of the membrane synthesized on the mullite support at 368 K for 6 h measured by EDX was ~2.9 (NaY type), and this membrane was selected as a promising FAU membrane for gas separation.

It is worth noting that membranes supported by mullite were thicker and had higher Si/Al ratios than that of membranes supported by α-Al_2O_3, which was plausibly attributed to the silicon element contained in mullite providing silicon-nutrient for the growth of FAU membranes.

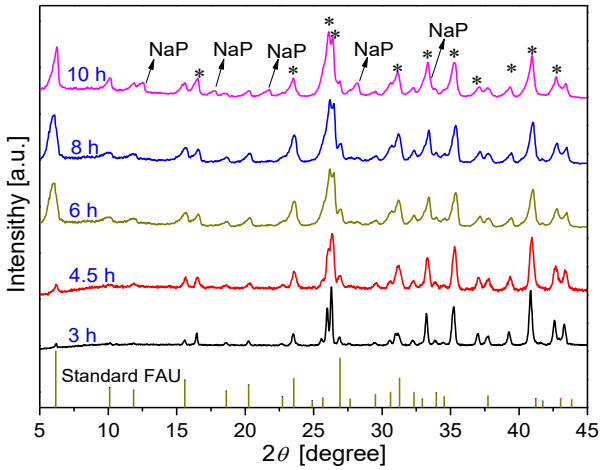

Figure 8. XRD patterns of FAU zeolite membranes synthesized on mullite supports at 368 K for different crystallization times (*: mullite support).

Preprints (www.preprints.org) | NOT PEER-REVIEWED | Posted: 19 October 2023 doi:10.20944/preprints202310.1150.v1

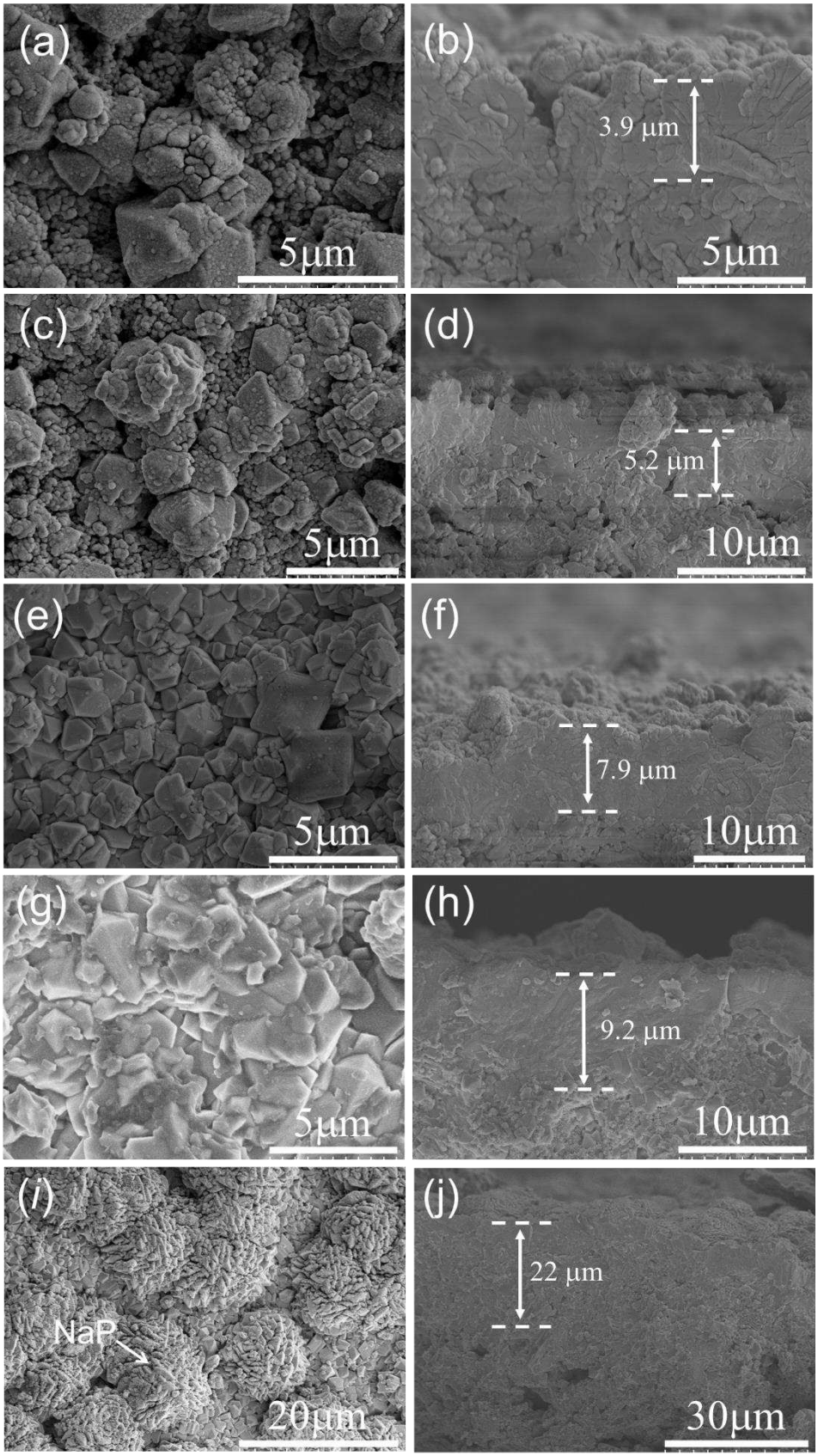

Figure 9. Surface and cross-sectional SEM images of FAU zeolite membranes with different crystallization times on mullite supports. (a, b) 3 h, (c, d) 4.5 h, (e, f) 6 h, (g, h) 8 h, (i, f) 10 h.

Preprints (www.preprints.org) | NOT PEER-REVIEWED | Posted: 19 October 2023 doi:10.20944/preprints202310.1150.v1

3.3. Gas separation performance

Based on the characteristics described thus far, two types of FAU (NaY) membranes with continuous, uniform, dense zeolite layers, that is, α-Al_2O_3-supported membranes (hereafter referred to as MA-*x*) synthesized at 368K for 8 h and mullite-supported membranes (hereafter referred to as MM-*x*) synthesized at 368K for 6 h, were selected as promising FAU membranes for gas separation.

3.3.1. Gas permeation

Figure 10 shows the single-gas permeance for H_2, CO_2, N_2, CH_4, C_3H_6, C_3H_8, and *i*-butane (*i*-C_4H_{10}) as a function of the kinetic diameter at room temperature through the MA-1 and MM-1 membranes. The permeances for the gases through both membranes decreased with the kinetic diameter of molecules except for CO_2 and N_2, and the permeance order was H_2 > CH_4 > C_3H_6 > C_3H_8 > *i*-C_4H_{10}. This is because the permeation of small-sized molecules (e.g., H_2, CO_2, N_2, and CH_4) through the FAU (pore size: 0.74 nm) membrane is mainly controlled by Knudsen diffusion, which is inversely proportional to the square root of the molecular weight ratio of the gases. However, the behavior of large-sized molecules permeating the membrane results from the combined effects of Knudsen diffusion, affinity (e.g., C_3H_6), and molecular sieving (e.g., *i*-C_4H_{10}). The H_2 permeance of the MA-1 membrane was as high as 5.34×10^{-7} mol/(m² s Pa), which is 3.4 times that of the MM-1 membrane. In addition, the H_2/C_3H_8 selectivity of the MA-1 membrane was 183, 10.1 times that of the MM-1 membrane, and the H_2/i-C_4H_{10} selectivity was as high as 315, 6.8 times that of the MM-1 membrane. The results demonstrate that compared to the MM-1 membrane, the MA-1 membrane layer was thinner without defects, reducing permeation resistance and maintaining high selectivity. It is worth noting that the C_3H_6/C_3H_8 selectivity of the MA-1 membrane was as high as 46, coupled with a remarkably high C_3H_6 permeance of 1.35×10^{-7} mol/(m² s Pa). In this work, both types of synthesized membranes had excellent selectivity for propylene/propane; that is, the permeance of propylene was higher than that of propane. This is because the propylene molecule has a smaller dynamic diameter, and there is a suitable electrostatic force between FAU (NaY) zeolite and the double bond of propylene, promoting propylene molecule permeation [37,38].

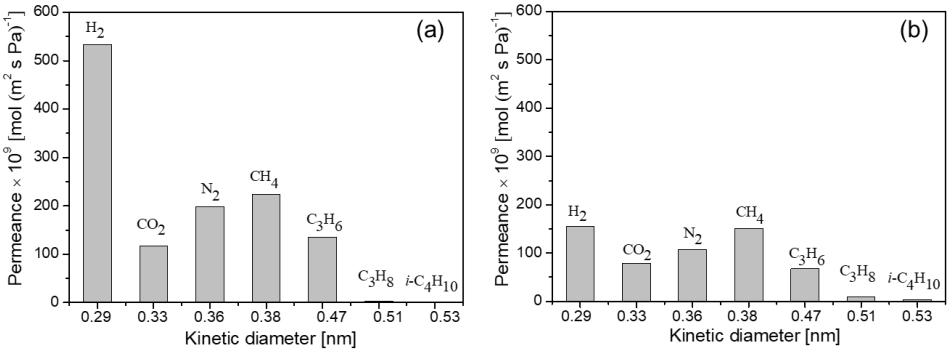

Figure 10. Single-gas permeance as a function of kinetic diameter at room temperature through (a) MA-1 (on the α-Al_2O_3 support) and (b) MM-1 (on the mullite support) membranes.

3.3.2. Membrane reproducibility

More than 3 FAU membranes were re-prepared for each type (i.e., MA and MM), and their gas separation performance was compared to confirm the reproducibility of the membranes, as listed in Table 1. Examination of all data, each type exhibited similar levels of permeability and selectivity. The relative standard deviations of permeance and selectivity were maintained within 14.8%, demonstrating that the membranes are reproducible [3].

Preprints (www.preprints.org) | NOT PEER-REVIEWED | Posted: 19 October 2023 doi:10.20944/preprints202310.1150.v1

Table 1. Gas separation performance for FAU (MA and MM) membranes prepared under the optimized conditions.

Membrane	Permeances [×10^{-7} mol (m^2 s Pa)$^{-1}$]		Selectivity		
	H_2	C_3H_6	H_2/C_3H_8	H_2/i-C_4H_{10}	C_3H_6/C_3H_8
MA-1	5.34	1.35	183	315	46
MA-2	5.11	1.22	176	309	42
MA-3	4.82	1.01	188	324	39
MM-1	1.55	0.68	18	46	7.9
MM-2	1.81	0.79	15	39	6.5
MM-3	1.50	0.59	14	44	5.5
Average for MA	5.09 ± 0.21	1.19 ± 0.14	182 ± 5	316 ± 6	42.3 ± 2.87
Average for MM	1.62 ± 0.14	0.68 ± 0.08	16 ± 2	43 ± 3	6.6 ± 0.98

3.3.3. Comparing gas separation performance with literature data

Substantial efforts have been made to develop high-performance zeolite membranes for gas separation. The H_2/C_3H_8 and C_3H_6/C_3H_8 separations are the most important and attractive processes in the petrochemical industry. For example, the products of direct dehydrogenation of propane to propylene (such as the Oleflex process) include abundant H_2, C_3H_6, and C_3H_8 [39]. The membrane needs to have good H_2/C_3H_8 and C_3H_6/C_3H_8 selectivity to achieve efficient separation and purification of the products. Figure 11 summarizes the separation performances of H_2/C_3H_8 and C_3H_6/C_3H_8 using FAU (MA-1) membrane synthesized on the α-Al_2O_3 support together with the membranes reported in recent years, which include polymer, silica, carbon, mixed matrix, and zeolite membranes (details are shown in Tables S1 and S2). Obviously, the MA-1 membrane has demonstrated attractive separation performance for H_2/C_3H_8 (H_2 permeance= 5.34 × 10^{-7} mol (m^2 s Pa)$^{-1}$, selectivit = 183) and C_3H_6/C_3H_8 (C_3H_6 permeance= 1.35 × 10^{-7} mol (m^2 s Pa)$^{-1}$, selectivity= 46). It is worth mentioning that compared with various types of membranes, the C_3H_6/C_3H_8 separation performance of the MA-1 membrane far surpasses their upper boundaries of the "tradeoff" line. The impressive gas separation capability was attributed to the thin membrane layer, defect-free, and high quality of the as-prepared FAU membrane (The optical photograph of the membrane is shown in Figure S1).

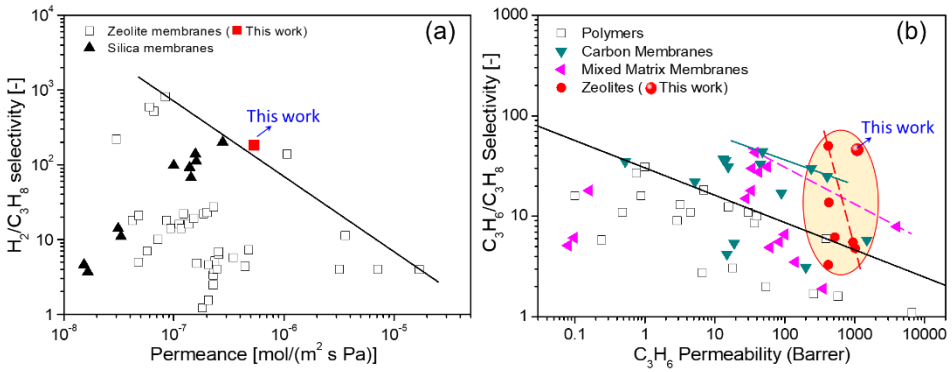

Figure 11. Comparing the separations of (a) H_2/C_3H_8 and (b) C_3H_6/C_3H_8 for gas separation membranes (Original data are shown in Tables S1 and S2).

4. Conclusions

In this study, high-performance FAU (NaY type) zeolite membranes were successfully synthesized using small-sized seeds of 50 nm, and their gas separation performance was evaluated. The results illustrated that further extending the crystallization time or increasing the synthesis temperature led to the formation of a NaP impurity phase on the FAU membrane layer. The most promising FAU membrane with a thickness of 2.7 μm was synthesized on an α-Al_2O_3 support at 368 K for 8 h, and had good reproducibility. The H_2 permeance of the membrane was as high as 5.34×10^{-7} mol/(m^2 s Pa), and the H_2/C_3H_8 and H_2/i-C_4H_{10} selectivities were 183 and 315, respectively. The most

attractive performance was that the C_3H_6/C_3H_8 selectivity of the membrane was as high as 46 with a remarkably high C_3H_6 permeance of 1.35×10^{-7} mol/(m^2 s Pa). The excellent separation performance of the membrane is mainly attributed to the thin, defect-free membrane layer and relatively wide pore size.

Supplementary Materials: The following supporting information can be downloaded at the website of this paper posted on Preprints.org.

Author Contributions: Writing—original draft preparation, investigation, Q.W.; Data curation, H.Y.C.; Data curation, F.Y.H.; Data curation, Q.L.; Data curation, review & editing, N.X.; Data curation, L.F.; Data curation, C.Y.W.; Data curation, L.Y.Z.; Review & editing, supervision, R.F.Z. All authors have read and agreed to the published version of the manuscript.

Funding: This work was supported by the National Natural Science Foundation of China (22308076), the Anhui Provincial Natural Science Foundation (2308085QB65), the University Natural Sciences Research Project of Anhui Province (KJ2021A1015, 2023AH040305), Key Research and Development Project of Anhui Province (2022a05020041), the Anhui Province Excellent Research and Innovation Team Project for Universities (2023AH010050), the Natural Science Foundation of Jiangsu Province (BK20220002), State Key Laboratory of Materials-Oriented Chemical Engineering (KL21-04), and the Talent Scientific Research Foundation of Hefei University (20RC33, 21-22RC36).

Conflicts of Interest: The authors declare no conflict of interest.

References

1. Sholl, D.S.; Lively, R.P. Seven chemical separations to change the world. *Nature* **2016**, *532*, 435-437.
2. Shrestha, S.; Dutta, P.K. Modification of a continuous zeolite membrane grown within porous polyethersulfone with Ag (I) cations for enhanced propylene/propane gas separation. *Microporous and Mesoporous Materials* **2019**, *279*, 178-185.
3. Wang, Q.; Wu, A.; Zhong, S.; Wang, B.; Zhou, R. Highly (*h0h*)-oriented silicalite-1 membranes for butane isomer separation. *Journal of Membrane Science* **2017**, *540*, 50-59.
4. Ren, Y.; Liang, X.; Dou, H.; Ye, C.; Guo, Z.; Wang, J.; Pan, Y.; Wu, H.; Guiver, M.D.; Jiang, Z. Membrane-based olefin/paraffin separations. *Advanced Science* **2020**, *7*, 2001398.
5. Sandru, M.; Sandru, E.M.; Ingram, W.F.; Deng, J.; Stenstad, P.M.; Deng, L.; Spontak, R.J. An integrated materials approach to ultrapermeable and ultraselective CO_2 polymer membranes. *Science* **2022**, *376*, 90-94.
6. Xia, Y.; Cao, H.; Xu, F.; Chen, Y.; Xia, Y.; Zhang, D.; Dai, L.; Qu, K.; Lian, C.; Huang, K. Polymeric membranes with aligned zeolite nanosheets for sustainable energy storage. *Nature Sustainability* **2022**, *5*, 1080-1091.
7. Wang, N.; Dang, G.; Bai, Z.; Wang, Q.; Liu, B.; Zhou, R.; Xing, W. In Situ Synthesis of Cation-Free Zirconia-Supported Zeolite CHA Membranes for Efficient CO_2/CH_4 Separation. *ACS Applied Materials & Interfaces* **2023**, *15*, 16853-16864.
8. Huang, W.; He, Z.; Liu, B.; Wang, Q.; Zhong, S.; Zhou, R.; Xing, W. Large surface-to-volume-ratio and ultrahigh selectivity SSZ-13 membranes on 61-channel monoliths for efficient separation of CO_2/CH_4 mixture. *Separation and Purification Technology* **2023**, *311*, 123285.
9. Wei, R.; Liu, X.; Zhou, Z.; Chen, C.; Yuan, Y.; Li, Z.; Li, X.; Dong, X.; Lu, D.; Han, Y. Carbon nanotube supported oriented metal organic framework membrane for effective ethylene/ethane separation. *Science Advances* **2022**, *8*, eabm6741.
10. Basel, N.; Liu, Q.; Fan, L.; Wang, Q.; Xu, N.; Wan, Y.; Dong, Q.; Huang, Z.; Guo, T. Surface charge enhanced synthesis of TpEB-based covalent organic framework (COF) membrane for dye separation with three typical charge properties. *Separation and Purification Technology* **2022**, *303*, 122243.
11. Liu, Q.; Basel, N.; Li, L.; Xu, N.; Dong, Q.; Fan, L.; Wang, Q.; Ding, A.; Wang, T. Interfacial polymerization of a covalent organic framework layer on titanium dioxide@ graphene oxide/polyacrylonitrile mixed-matrix membranes for high-performance dye separation. *Journal of Membrane Science* **2022**, *647*, 120296.
12. Tong, H.; Liu, Q.; Xu, N.; Wang, Q.; Fan, L.; Dong, Q.; Ding, A. Efficient Pervaporation for Ethanol Dehydration: Ultrasonic Spraying Preparation of Polyvinyl Alcohol (PVA)/Ti_3C_2Tx Nanosheet Mixed Matrix Membranes. *Membranes* **2023**, *13*, 430.
13. Wang, Q.; Zhou, R.; Tsuru, T. Recent Progress in Silicon Carbide-Based Membranes for Gas Separation.

Membranes **2022**, *12*, 1255.

14. Wang, Q.; Xu, N.; Liu, Q.; Dong, Q.; Nagasawa, H.; Kanezashi, M.; Zhou, R.; Tsuru, T. Low-temperature cross-linking fabrication of sub-nanoporous SiC-based membranes for application to the pervaporation removal of methanol. *Journal of Membrane Science* **2022**, *662*, 121008.
15. Yu, X.; Wang, Q.; Nagasawa, H.; Kanezashi, M.; Tsuru, T. SiC mesoporous membranes for sulfuric acid decomposition at high temperatures in the iodine–sulfur process. *RSC Advances* **2020**, *10*, 41883-41890.
16. Shao, J.; Ge, Q.; Shan, L.; Wang, Z.; Yan, Y. Influences of seeds on the properties of zeolite NaA membranes on alumina hollow fibers. *Industrial & engineering chemistry research* **2011**, *50*, 9718-9726.
17. Zhou, C.; Zhou, J.; Huang, A. Seeding-free synthesis of zeolite FAU membrane for seawater desalination by pervaporation. *Microporous and Mesoporous Materials* **2016**, *234*, 377-383.
18. Zhou, J.; Zhou, C.; Xu, K.; Caro, J.; Huang, A. Seeding-free synthesis of large tubular zeolite FAU membranes for dewatering of dimethyl carbonate by pervaporation. *Microporous and Mesoporous Materials* **2020**, *292*, 109713.
19. Zhou, C.; Yuan, C.; Zhu, Y.; Caro, J.; Huang, A. Facile synthesis of zeolite FAU molecular sieve membranes on bio-adhesive polydopamine modified Al_2O_3 tubes. *Journal of membrane science* **2015**, *494*, 174-181.
20. Xia, B.; Wang, S.; Li, B.; Cao, Y.; Liu, T.; Gao, P.; Chen, C.; Li, Y. Seeding-free synthesis of FAU-type membrane with dry gel modified α-alumina support. *Microporous and Mesoporous Materials* **2021**, *323*, 111219.
21. Nazir, L.S.M.; Yeong, Y.F.; Chew, T.L. Methods and synthesis parameters affecting the formation of FAU type zeolite membrane and its separation performance: a review. *Journal of Asian Ceramic Societies* **2020**, *8*, 553-571.
22. Nazir, L.S.M.; Yeong, Y.F.; Chew, T.L. Study on the effect of seed particle size toward the formation of NaX zeolite membranes via vacuum-assisted seeding technique. *Journal of Asian Ceramic Societies* **2021**, *9*, 586-597.
23. Gu, X.; Dong, J.; Nenoff, T.M. Synthesis of defect-free FAU-type zeolite membranes and separation for dry and moist CO_2/N_2 mixtures. *Industrial & engineering chemistry research* **2005**, *44*, 937-944.
24. Holmberg, B.A.; Wang, H.; Norbeck, J.M.; Yan, Y. Controlling size and yield of zeolite Y nanocrystals using tetramethylammonium bromide. *Microporous and mesoporous materials* **2003**, *59*, 13-28.
25. Wang, Q.; Yu, L.; Nagasawa, H.; Kanezashi, M.; Tsuru, T. High-performance molecular-separation ceramic membranes derived from oxidative cross-linked polytitanocarbosilane. *Journal of the American Ceramic Society* **2020**, *103*, 4473-4488, doi:10.1111/jace.17108.
26. Wang, Q.; Kawano, Y.; Yu, L.; Nagasawa, H.; Kanezashi, M.; Tsuru, T. Development of high-performance sub-nanoporous SiC-based membranes derived from polytitanocarbosilane. *Journal of Membrane Science* **2020**, *598*, 117688, doi:10.1016/j.memsci.2019.117688.
27. Wang, Q.; Yu, L.; Nagasawa, H.; Kanezashi, M.; Tsuru, T. Tuning the microstructure of polycarbosilane-derived SiC(O) separation membranes via thermal-oxidative cross-linking. *Separation and Purification Technology* **2020**, *248*, 117067.
28. Wang, Q.; Yokoji, M.; Nagasawa, H.; Yu, L.; Kanezashi, M.; Tsuru, T. Microstructure evolution and enhanced permeation of SiC membranes derived from allylhydridopolycarbosilane. *Journal of Membrane Science* **2020**, *612*, 118392.
29. Zhou, R.; Zhang, Q.; Shao, J.; Wang, Z.; Chen, X.; Kita, H. Optimization of NaY zeolite membrane preparation for the separation of methanol/methyl methacrylate mixtures. *Desalination* **2012**, *291*, 41-47.
30. Kumakiri, I.; Yamaguchi, T.; Nakao, S.-i. Preparation of zeolite A and faujasite membranes from a clear solution. *Industrial & engineering chemistry research* **1999**, *38*, 4682-4688.
31. Zhu, F.; Landon, J.; Liu, K. FAU zeolite membranes for dewatering of amine-based post-combustion CO_2 capture solutions. *AIChE Journal* **2020**, *66*, e17042.
32. Okamoto, K.-i.; Kita, H.; Horii, K.; Kondo, K.T. Zeolite NaA membrane: preparation, single-gas permeation, and pervaporation and vapor permeation of water/organic liquid mixtures. *Industrial & engineering chemistry research* **2001**, *40*, 163-175.
33. Lucero, J.M.; Crawford, J.M.; Wolden, C.A.; Carreon, M.A. Tunability of ammonia adsorption over NaP zeolite. *Microporous and Mesoporous Materials* **2021**, *324*, 111288.
34. Lang, W.-Z.; Ouyang, J.-X.; Guo, Y.-J.; Chu, L.-F. Synthesis of tubular faujasite X-type membranes with mullite supports and their gas permeances for N_2/CO_2 mixtures. *Separation Science and Technology* **2011**, *46*, 1716-1725.

35. Wang, B.; Sun, C.; Zhou, R.; Xing, W. A super-permeable and highly-oriented SAPO-34 thin membrane prepared by a green gel-less method using high-aspect-ratio nanosheets for efficient CO_2 capture. *Chemical Engineering Journal* **2022**, *442*, 136336.
36. Zhang, H.; Yang, Y.; Wang, Z. Synthesis of hierarchical LTA zeolite membranes by vapor phase transformation. *Journal of Membrane Science* **2023**, *671*, 121391.
37. Mundstock, A.; Wang, N.; Friebe, S.; Caro, J. Propane/propene permeation through Na-X membranes: The interplay of separation performance and pre-synthetic support functionalization. *Microporous and Mesoporous Materials* **2015**, *215*, 20-28.
38. Van Miltenburg, A.; Gascon, J.; Zhu, W.; Kapteijn, F.; Moulijn, J.A. Propylene/propane mixture adsorption on faujasite sorbents. *Adsorption* **2008**, *14*, 309-321.
39. Carter, J.H.; Bere, T.; Pitchers, J.R.; Hewes, D.G.; Vandegehuchte, B.D.; Kiely, C.J.; Taylor, S.H.; Hutchings, G.J. Direct and oxidative dehydrogenation of propane: from catalyst design to industrial application. *Green Chemistry* **2021**, *23*, 9747-9799.